International Journal of Automation and Computing

DOI: 10.1007/s11633-017-1103-x

Feedforward Control for Wind Turbine Load Reduction with Pseudo-LIDAR Measurement

Jie Bao [1] Hong Yue [1] William E. Leithead [1] Ji-Qiang Wang [2]

[1] Department of Electronic and Electrical Engineering, University of Strathclyde, Glasgow, G1 1XW, UK

[2] Jiangsu Province Key Laboratory of Aerospace Power System, Nanjing University of Aeronautics and Astronautics, Nanjing 210016, China

Abstract: A gain-scheduled feedforward controller, based on pseudo-LIDAR (light detection and ranging) wind speed measurement, is designed to augment the baseline feedback controller for wind turbine′s load reduction in above rated operation. The pseudo-LIDAR measurement data are generated from a commercial software Bladed using a designed sampling strategy. The nonlinear wind turbine model has been simplified and linearised at a set of equilibrium operating points. The feedforward controller is firstly developed based on a linearised model at an above rated wind speed, and then expanded to the full above rated operational envelope by employing gain scheduling strategy. The combined feedforward and baseline feedback control is simulated on a 5 MW industrial wind turbine model. Simulation studies demonstrate that the proposed control strategy can improve the rotor and tower load reduction performance for large wind turbines.

Keywords: Wind turbine control, light detection and ranging (LIDAR) measurement, feedforward control, load reduction, gain scheduling, disturbance rejection.

1 Introduction

1.1 Wind turbine load rejection strategies

With the increase of installed wind power capacity over the past few years, operation and maintenance of wind energy production becomes a critical issue in wind industry. Conventional wind turbine control systems employ feedback control schemes involving proportional-integral-derivative/proportional integral (PI/PID) controllers[1]. The main control objectives are to maximise the energy capture in below rated operation and maintain the power output at its rated level in above rated operation. As the size of wind turbines has increased, the demands on controller have increased especially on reduction of structural loads. It is always a challenging task to achieve good load reduction without compromising energy capture performance.

The mechanical loads on a wind turbine are mainly caused by the interaction between the turbine and the wind field experienced by the turbine. It includes the structural loads which are due to impacts from the wind to the turbine structure, and the drive-train loads which are the loads that propagate down to the drive-train components[2, 3]. The structural loads mainly include loads on tower, blades, hub, etc. The usual approach to reduce tower loads is to augment the pitch demand by an additive adjustment in response to a measurement of the tower head fore-and-aft velocity or acceleration. Options include introducing a tower feedback loop[4, 5], or the coordinated control strategy that combines pitch and torque demand in above rated conditions[6, 7]. In large wind turbines, each blade has its own actuator capable of adjusting the blade to the demanded pitch angle. The standard collective pitch control provides the same demand on all three blades which cannot reduce unbalanced loads on the rotor. To deal with this unbalance in loads, each blade must be pitched independently. For this purpose, individual pitch control and individual blade control have been developed[8, 9], both providing additive adjustment to the demanded pitch angle from the basic speed controller.

With the above load reduction approaches based on feedback control scheme, the loads can only be controlled once their influences on the turbine are induced. In other words, there is always a delay between the load impact and the controller response. A possible solution to this problem is to employ the incoming wind disturbance information into the control system in advance so that the controller can respond to the disturbance and thereby alleviate the induced loads timely. This method depends on direct and accurate wind measurement to estimate the disturbance.

In traditional wind measurement for individual turbines, a wind anemometer is mounted on top of the na-

Research Article

Special Issue on Automation and Computing Advancements for Future Industries

Manuscript received February 16, 2017; accepted September 28, 2017

This work was supported by UK Engineering and Physical Sciences Research Council (EPSRC) Supergen Wind project (No. EP/N006224/1)

Recommended by Guest Editor Zhi-Jie Xu

celle. This measurement of wind speed cannot be used directly in wind turbine control because it only indicates a point wind speed at a fixed position. A more recent measurement technology, light detection and ranging (LIDAR), has been developed to measure wind speed over a distance and covering a wide space, which makes it possible to exploit the incoming wind speed information in the turbine control system.

The main benefits from LIDAR include the following.

1) Preview and accurate wind speed measurement

For individual wind turbine, either a wind anemometer or a LIDAR device is generally mounted on the nacelle. The wind anemometer can only measure the wind at its own position which is normally behind the turbine rotor. In this case, the wind has already interacted with the turbine before it is measured by the anemometer. This wind speed information is therefore "delayed" and is not suitable for controller design. Moreover, the incoming wind field would be significantly affected after it is experienced by the rotating rotor blades, known as the wake effect, which will reduce the measurement accuracy of the anemometer.

Comparing to the wind anemometer, a LIDAR device can emit laser beams to the front of the turbine and therefore measure and provide the incoming wind speed information before the wind reaches the turbine. This allows extra time for the controller to make a response.

2) Spatial distributional wind speed measurement

Instead of the conventional single point wind speed measurement, LIDAR can measure the incoming wind field over a spatial distribution through its scanning pattern. This is particularly significant for large wind turbines. The rotor diameters of modern large wind turbines are generally at a hundred-meter level. Consideration of wind speed distribution across such a large rotor plane area is necessary to evaluate the wind-induced rotor dynamics on the wind turbine.

Information on LIDAR basics can be found in recent literature, for example, LIDAR configurations and turbine-mounted options[10, 11], data analyses from LIDAR measurement[12], field testing studies[11, 13].

1.2 LIDAR measurement in wind turbine control

LIDAR-based feedforward control has been proposed as complementary to the baseline control system so as to enhance the above rated pitch control performance. The initial attempts focus on the design of independent feedforward controllers which enable the wind information as an input to the controllers and thereby compensate the wind disturbances in the control system. The proposed methods include the use of basic feedforward schemes for collective pitch control[14–16] and individual pitch control[17], in which the wind speed measurement is provided or supposed to be provided by LIDAR, and some advanced feedforward control algorithms such as feedforward control with non-causal series expansion approximation[18], H-infinity preview control[19], and adaptive control[20] have been developed. Potential improvements on reducing the turbine loads and pitch control actions in above rated operation have been discussed on these LIDAR assisted feedforward control strategies.

Advanced control techniques such as model-based predictive control (MPC) employing wind speed measurement has also been investigated, in which the future events of the wind turbine based on the preview wind measurement are predicted for a better wind disturbance rejection response of the controller. Both linear methods[21, 22] and nonlinear algorithms[23] are applied. Field testing studies have been presented for both feedforward control[24, 25] and MPC[26].

Apart from the work on load reduction in above rated condition by LIDAR-assisted control design, the energy capture performance in below rated conditions[27, 28] and the consideration of LIDAR measurement in controlling the yaw movements[29] are also investigated. However, the results suggest that LIDAR-assisted control has limited improvements in energy capture and yaw control performances in below rated operation, but requires more control actions. Therefore, applying LIDAR measurements for above rated pitch control could be more beneficial.

To make effective use of LIDAR information for control system development, it is important to implement LIDAR measurement and process LIDAR data properly. In an analysis of the raw LIDAR measurement data, several types of LIDAR measurement errors are introduced and the methods to exclude part of these errors are also suggested[30]. While modelling of wind evolution process is a topic of most interest[31–34], other aspects of LIDAR measurement errors/inaccuracies are also discussed and investigated[35–37].

Motivated by the recent development of LIDAR in wind turbine control, in this work, a LIDAR-assisted feedforward controller is developed for nonlinear large-scale wind turbines with the aim to reduce load effectively. Different from a preliminary design[38], in this work, the controller is developed based on a set of linearised models, which allows control in above rated operation and also the transition region, i.e., the region between below-rated and above-rated. A stable inversion of the turbine dynamics is included in the controller design to ensure the system stability when dealing with the unstable zeros in the turbine model. Control implementations in the transition region and at high wind speed are simulated with realistic turbulent wind speeds. The rest of the paper is organised as follows. In Section 2, the pseudo-LIDAR data production with a designed sampling strategy is introduced. Linearised models are developed and validated for the controller design. Section 3 gives the design details on the gain-scheduling feedforward control method. Simulation studies on a 5 MW machine are presented in Section 4, and conclusions are given in Section 5.

2 Generation of LIDAR data and wind turbine modelling

2.1 Pseudo-LIDAR data generation

In this work, the LIDAR measurement data used for simulation are produced from the commercial software – Bladed. This powerful tool can model a three-dimensional turbulent wind field. The cubic structure consists of a number of points that are uniformly distributed inside the model, as depicted in Fig. 1. Each point in the model contains wind speed information including the longitudinal, lateral and vertical components. To simplify the terminology, we use X, Y and Z to denote these three components respectively. Thus, the model is defined in an X-Y-Z coordinate system.

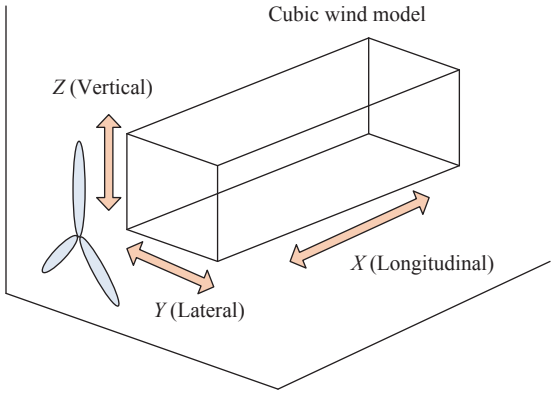

Fig. 1 Wind field construction in Bladed settings

In the model as shown in Fig. 1, wind speed variations for the points along the X axis are regarded as the time variations of wind speed in a fixed position. Therefore, all the point wind speed time variations at the Y-Z plane can be obtained by the point wind speed spatial variations along the X axis. Since the Y-Z plane covers the area of the turbine rotor, this plane can be defined as the rotor plane. Consequently, all the point wind speeds at the rotor plane can be obtained.

In Bladed, the wind model is generated using Veers method[39], in which the turbulence structure is isotropic. In this structure, the correlations between each point along the three components are identical and thereby one of the three components can be represented by the other two components. Based on this property, a new sampling strategy is designed to reconstruct the wind model. With the default settings in Bladed, the X axis is defined as the time axis and also the wind field incoming direction, which is perpendicular to the turbine rotor plane. In the newly designed strategy, the time axis is still represented by the X axis, but the wind incoming direction is selected to be defined on the Y axis. As a result, the X-Z planes in the cubic structure represent the planes which are parallel to the rotor plane, as shown in Fig. 2.

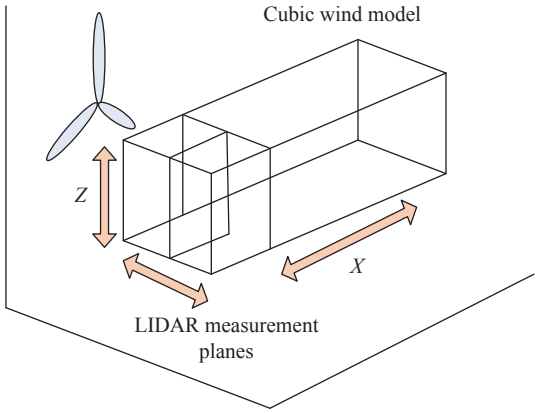

Fig. 2 Reconstructed wind speed sampling model with pseudo-LIDAR measurement

In Fig. 2, the leftmost X-Z plane is defined as the rotor plane, thus the other X-Z planes selected along the Y axis are defined as the LIDAR scanning planes with different distances to the rotor plane, which can thereby provide the incoming wind profile information at different positions. Therefore, in this reconstructed wind model, the points along the Y axis represent the positions with some distances to the turbine rotor, and the wind speed variations in time domain are represented by the point speeds along the X axis. The spatial interval between the points along the X axis is defined as the time intervals. If a set of points are selected from each X-Z plane, i.e., the rotor plane and LIDAR measurement plane, the wind speed time series data for each point will be different. This is to reflect the wind evolution from the measurement location to the turbine.

Using the above sampling method to create pseudo-LIDAR measurement data, eight X-Z planes are selected along the Y axis with equal distance between each other. The first plane represents the rotor plane, the other seven planes represent the LIDAR measurement planes at distances of 14.285 7 m, 28.571 4 m, 42.857 1 m, 57.142 8 m, 71.428 5 m, 85.714 2 m and 100 m, respectively, from the rotor plane. The point wind speeds distributed over the plane are averaged to represent the effective wind speed at that plane position. In this way, the rotor wind speed data and the LIDAR measurement data can be obtained.

In order to present the wind evolution property, the correlations between rotor wind speed and each LIDAR measurement are firstly examined. Figs. 3 and 4 illustrate the auto-spectrum of the wind speed data series for each LIDAR measurement plane and the cross-spectrum between the rotor wind speed and the other seven LIDAR wind speed series. The wind speed is generated with a mean value of 20 m/s and a turbulence intensity of 5% in this simulation. Auto-spectrum and cross-spectrum will be used to approximate the wind evolution model later on.

It should be noted that the pseudo-LIDAR data used in this work is taken as perfect measurement of the incoming wind field. With real LIDAR measurement, the

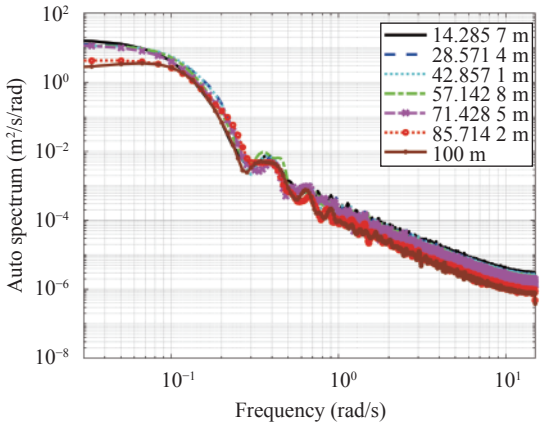

Fig. 3 Auto-spectrums for each LIDAR measurement

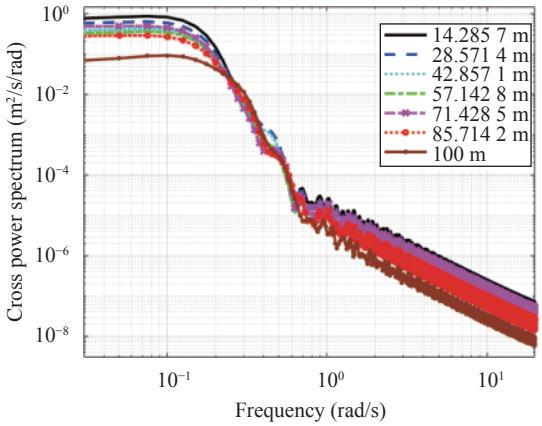

Fig. 4 Cross-spectrums between rotor and each LIDAR measurement

measured wind speed data contain measurement errors. For example, a LIDAR device emits laser beams to scan the small particles in the wind field in front of the wind turbine. These laser beams will then be backscattered and received by the LIDAR device. According to the Doppler frequency shift between the emitted and backscattered laser beams, the moving speed of the small particles, which is believed to be equivalent to the wind speed, can thereby be calculated. However, due to the line-of-sight (LOS) measurement of LIDAR, this wind speed is actually the wind speed component in the direction of the laser beam, rather than the wind speed perpendicular to the wind turbine rotor plane. Therefore, this error caused by the LIDAR LOS measurement must be processed. Another assumption to avoid such error is to use more LIDAR devices to scan the same focus point simultaneously. This would help to obtain more information of the incoming wind field and hence the correct wind speed.

2.2 Baseline wind turbine model

A 5 MW Supergen exemplar wind turbine model developed at Strathclyde University in Simulink is used as the baseline model for controller design and simulations. The basic turbine parameters are:

1) Rotor radius: 63 m
2) Hub height: 90 m
3) Gearbox ratio: 97
4) Minimum generator speed: 70 rad/s
5) Maximum generator speed: 120 rad/s
6) Cut-in wind speed: 4 m/s
7) Cut-out wind speed: 25 m/s
8) Rated wind speed: 11.9 m/s
9) Rated power: 5 MW.

This is a nonlinear model with fully established aerodynamics, drive-train dynamics and power generation unit dynamics. Details can be found in [40].

2.3 Linearisation of wind turbine model

The controller design in this work is based on linearised models at above rated wind speed operating points. A simplified wind turbine model includes the turbine dynamics briefed as follows. The relationship between the rotor speed and the torques is defined in (1).

$$I\dot{\Omega}+B\Omega = T_f - T_e \tag{1}$$

where I is the total inertia and Ω is the rotor speed. $B\Omega$ is the total viscous damping in the drive-train. T_f is the aerodynamic torque and T_e is the generator reaction torque. The aerodynamic torque is affected by the wind speed, rotor speed and the pitch angle, as shown in (2).

$$T_f = \frac{1}{2}\rho\pi V^2 R^3 \frac{C_p(\lambda,\beta)}{\lambda} \tag{2}$$

where ρ is the air density, R is the rotor radius, V is the wind speed and C_p is the power coefficient that is determined by the blade pitch angle β and the tip-speed ratio λ. The tip-speed ratio is then defined by $\lambda = \dfrac{\Omega R}{V}$.

The transfer functions linking the generator speed ω_g, the rotor speed Ω, the aerodynamic torque T_f, and the generator reaction torque T_e, are defined in (3).

$$\begin{bmatrix} \Omega \\ \omega_{\mathrm{g}} \end{bmatrix} = \begin{bmatrix} A(s) & B(s) \\ C(s) & D(s) \end{bmatrix} \begin{bmatrix} T_f \\ T_e \end{bmatrix} \tag{3}$$

where $A(s)$, $-\dfrac{B(s)}{N}$, $\dfrac{C(s)}{N}$, $-\dfrac{D(s)}{N^2}$ are reduced to (4) by ignoring the intermediate and high frequency components.

$$\frac{1}{Is+B} \tag{4}$$

where N is the gearbox ratio, I is the total inertia and B is the total viscous damping coefficient of the system.

Based on the nonlinear model provided above, the wind turbine model is linearised at the wind speed oper-

ating points of 12 m/s, 14 m/s, 16 m/s, 18 m/s, 20 m/s, and 22 m/s, respectively. The inputs for the linearised model are the generator torque, the wind speed and the pitch angle demand, the output is the generator speed.

2.4 Validation of linearised models

The linearised models from Simulink are compared with the linearised models generated by Bladed using the complex wind turbine model in Section 2.2. Figs. 5 and 6 present the frequency responses of the two linearised models, for transfer functions (TFs) from pitch demand to generator speed (subscript "pg" used in all figures), and from wind speed to generator speed (subscript "wg" used in all figures), respectively. The selected wind operating point is 12 m/s in Fig. 5, which is a wind speed close to the rated wind speed, and 20 m/s in Fig. 6, which is a high wind speed. It can be seen that the frequency responses from the two models match well in the frequency range of operating relevance. The Bladed linearised models have up to 20th order. Our simplified models have a lower order number of 7, which are less complex. These simplified linear models will be used for the controller design.

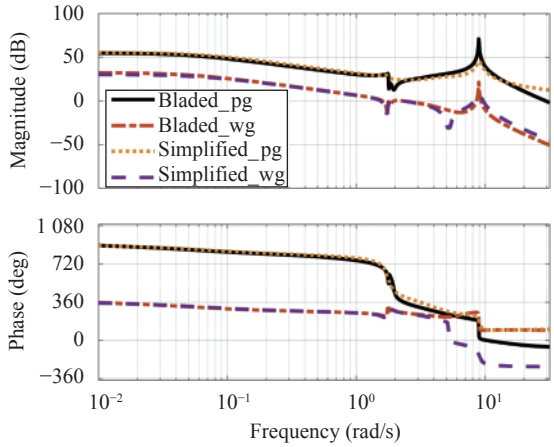

Fig. 5 Bode plot comparisons between the Bladed linearised model and the simplified linearised model. TFs from pitch demand to generator speed and from wind speed to generator speed, at the wind speed operating point of 12 m/s.

3 Feedforward control design

3.1 Baseline control system

A previously developed 5 MW wind turbine model is used for simulation study. The baseline control system included in the model consists of several main parts: the main speed controller including a below rated component of torque controller and an above rated component of pitch controller, the drive-train filter and the tower filter.

1) Below rated torque controller

A torque controller controlling the generator reaction torque in response to the generator speed is employed in

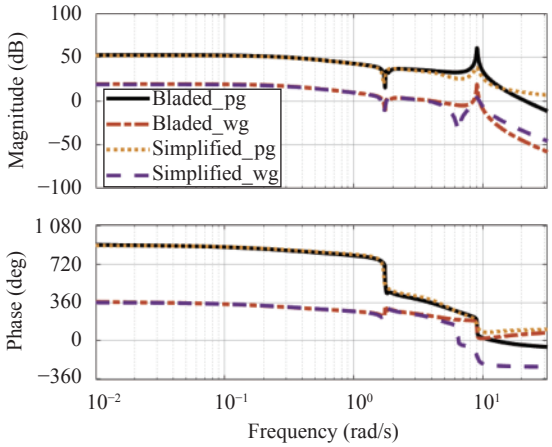

Fig. 6 Bode plot comparisons between the Bladed linearised models and the simplified linearised models. TFs from pitch demand to generator speed and from wind speed to generator speed, at the wind speed operating point of 20 m/s.

below rated operation, to follow the designed $C_P - \lambda$ tracking curve. The controller is designed to provide a bandwidth of at least 1 rad/s and has good high frequency roll off through loop shaping.

2) Above rated pitch controller

In above rated region, a pitch controller is employed to control the blade pitch angle in response to the generator speed. The pitch controller aims to maintain the power output at its rated level.

The aerodynamics of the wind turbine is highly nonlinear in above rated condition. When using linearised models obtained at equilibrium operating points, gain scheduling is employed based on the use of the separability characteristics of wind turbines. According to the separability theory, the nonlinear aerodynamics of the wind turbine can be divided into two independent parts as presented below.

$$T(\beta, \Omega, V) = h(\beta, \Omega) - g(V). \tag{5}$$

In (5), β, Ω, V denote the pitch angle, generator speed and the wind speed, respectively. T is the aerodynamic torque which is determined by β, Ω and V, which can be divided into two parts: the function $h(\cdot)$ that is dependent on β and Ω, and the function $g(\cdot)$ that is only dependent on V. In this way, the wind speed is taken as a separate disturbance term that does not affect the aerodynamic torque. A global gain scheduling technique is thus made possible. More details can be found in [41].

3) Drive-train filter

In addition to the main speed feedback controller, a drive-train filter is used to damp the drive-train mode at the drive-train frequency, as shown in Fig. 7.

The following band-pass filter is taken:

$$F(s) = \frac{k \times s}{s^2 + 2\eta \times \omega_{dtr} s + \omega_{dtr}^2} \tag{6}$$

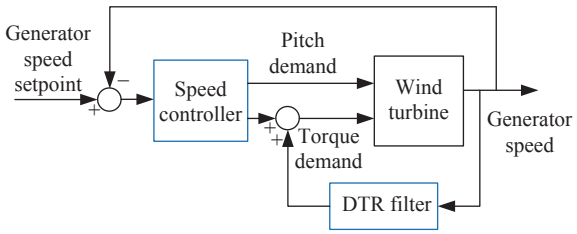

Fig. 7 Baseline speed feedback control with drive-train filter

where ω_{dtr} is the drive-train frequency at which we aim to design the filter to remove spikes in spectral response, η is a damping ratio that can be chosen at the value of 0.6. With this band-pass filter design, the drive-train mode damping can be achieved.

4) Tower filter

Similar to the drive-train filter, a tower feedback loop is added in response to the tower fore-aft acceleration which can be measured by an accelerometer in the nacelle (see Fig. 8). The filter is employed in above rated operation, which is designed to damp the first tower mode by adjusting the pitch angle. A typical transfer function for the tower filter is similar to (6). The tuning parameters are set up to increase tower motion damping at the first tower fore-aft mode.

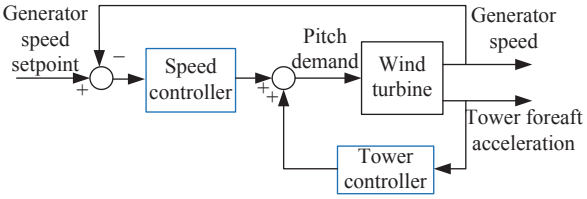

Fig. 8 Baseline tower feedback loop and speed feedback control

3.2 Feedforward controller design

In this work, a feedforward channel is added to the baseline speed controller, as shown in Fig. 9. The baseline controller includes all of the components described in Section 3.1. A feedforward controller is then developed to compensate the wind disturbance with the use of pseudo-LIDAR measurement.

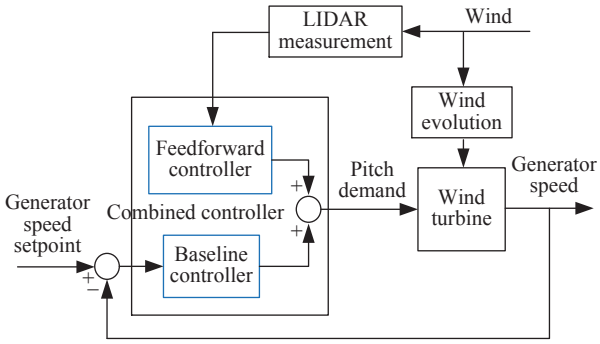

Fig. 9 Feedforward controller combined with baseline controller

In order to design the feedforward controller, the wind turbine model is firstly linearised at an above rated wind speed operating point as introduced in Section 2. Fig. 10 illustrates the block diagram of such a linear control scheme. The linearised turbine model consists of two components, denoted by G_1 and G_2 in the diagram. G_1 is the transfer function from the wind speed V, to the generator speed ω_o, and G_2 is the transfer function from the pitch demand β, to the generator speed ω_o. The transfer functions of the feedback pitch controller and the feedforward controller are represented by G_{FB} and G_{FF}, respectively. ω_{set} is the generator speed setpoint. G_L denotes the transfer function of LIDAR measurement and G_E denotes the wind evolution process from the LIDAR sensing position to the turbine rotor. Thus, for the system shown in Fig. 10, the relationship between the input and output can be described as

$$\omega_o = \frac{G_{FB}G_2}{1+G_{FB}G_2}\omega_{set} + \frac{G_EG_1 + G_LG_{FF}G_2}{1+G_{FB}G_2}V. \tag{7}$$

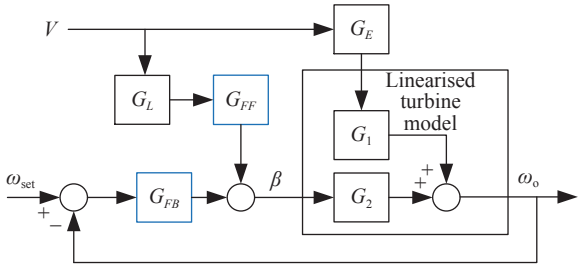

Fig. 10 Block diagram of the feedforward control system

Subsequently, to compensate the effect from the measured wind disturbance to the generator speed, the feedforward controller is designed to make the disturbance transfer function as 0, which requires

$$G_{FF} = -\frac{G_1G_E}{G_2G_L}. \tag{8}$$

Finally, the transfer function of the feedforward controller is obtained as shown in (9). G_1 and G_2 are known directly from the linearised turbine model. However, G_E and G_L are hard to be modelled, especially G_E which represents a very complex wind evolution process. Nevertheless, a transfer function representing the relationship between G_E and G_L can be estimated by a filter, which employs the auto-spectrum of the LIDAR wind speed S_A, and the cross-spectrum between the rotor wind speed and the LIDAR wind speed S_C[25]. This can be derived from the results in Section 2.1.

$$\frac{G_E}{G_L} = G_{EL} = \frac{S_C}{S_A}. \tag{9}$$

In addition, since the feedforward controller is designed mainly for load reduction in above rated conditions, the implementation in the transition region between the below rated and above rated should be taken into account to avoid redundant pitch actuation in below rated operation.

A switching scheme is developed to ensure the smooth switching in the transition region, as shown in Fig. 11.

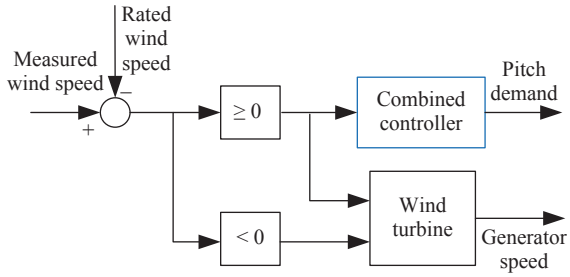

Fig. 11 Switching scheme in the transition region

3.3 Stable inversion of the turbine dynamics

As presented in the previous section, the calculation of the feedforward controller for any linearised models requires the inversion of the wind turbine dynamics, i.e., the inversion of the linearised turbine model G_2, from the pitch demand input to the generator speed output. However, G_2 contains positive zeros in the right half plane (RHP), known as the non-minimum phase zeros. When conducting the inverse calculation, these zeros would become RHP poles leading to an unstable system. In this section, a zero phase error tracking control (ZPETC) method[42] is used to obtain a stable inversion of the model. The method was originally developed based on a discrete-time control algorithm, while in this work, it is converted to a continuous-time version for the established turbine model and controller.

Denote the transfer function G_2 as shown in (10).

$$G_2(s) = \frac{B_s(s)B_u(s)}{A(s)} \tag{10}$$

where $A(s)$ represents the denominator, $B_u(s)$ is the numerator which contains all the unstable zeros and $B_s(s)$ contains all the stable zeros.

Ideally the wind disturbance can be compensated according to (7) and (8) where $G_2G_2^{-1}$=1. However, this cannot be directly achieved due to the unstable zeros in G_2. By applying the ZPETC method in continuous-time domain, a stable approximation of the inversed G_2 can be obtained,

$${G_2}^{-1}(s)^* = \frac{A(s)\,B_u(-s)}{B_s(s)\,[B_u(0)]^2}. \tag{11}$$

Again the new result of $G_2G_2^{-1^*}$ will not have an imaginary part, thus, there is no phase shift at all frequencies.

3.4 Gain scheduling

To handle the nonlinearities of the wind turbine model over the above rated operating range, gain scheduling is employed in developing the feedforward controller. Conventional gain scheduling methods include methods such as sliding mode control[43, 44] and linear parameter varying (LPV) control[45]. For convenience, a simple method is used instead in this feedforward controller design. For this turbine model, the rated wind speed is 11.9 m/s. Therefore, we design the feedforward controller at a given speed as discussed above, and then calculate the feedforward gain for each wind speed from 12 m/s to 22 m/s with an interval of 2 m/s. These feedforward gains are scheduled by applying a lookup table in implementation.

4 Simulation studies

The designed gain scheduling feedforward controller is applied to the 5 MW Supergen nonlinear wind turbine model. Simulations are conducted with Simulink. The combined feedforward control and the baseline feedback control is compared with the baseline controller. The control performance on the pitch actuator, rotor loads, tower loads and power output are assessed by relevant measures.

In the reference wind turbine model, the rotor blades are modelled as a whole, instead of being modelled individually for each blade. Therefore, in the simulation, the averaged blade root flapwise bending moment of the three blades, known as the out-of-plane rotor torque, is evaluated instead of the root bending moment on each blade. Similarly, the averaged blade root edgewise bending moment is evaluated, known as the in-plane rotor torque.

There are two sets of simulations, one employs a 12 m/s turbulent wind speed which corresponds to the transition region between the below and above rated operation, the other one employs a 20 m/s turbulent wind speed which represents the high wind speed region.

4.1 Transition region

A turbulent wind with mean wind speed of 12 m/s and turbulence intensity of 5% is used in the simulation, as shown in Fig. 12. The results are generated both in time domain and in frequency domain taking the measure of power spectral density (PSD).

In Fig. 13, reduction in the pitch rate can be observed from the results using the combined feedforward and feedback control. The reduction of pitch control actions implies an improvement for energy saving and lifetime ex-

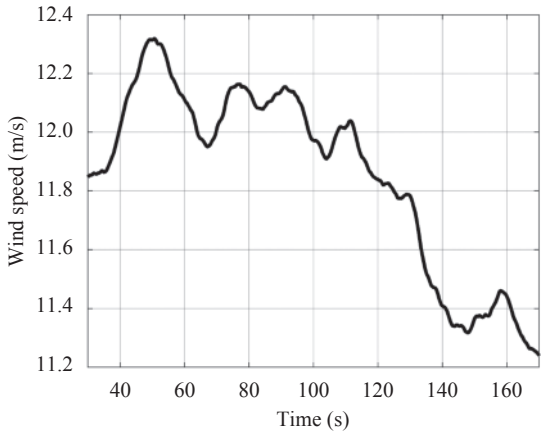

Fig. 12 Wind speed profile used in the transition region (mean wind 12 m/s, turbulence intensity 5%)

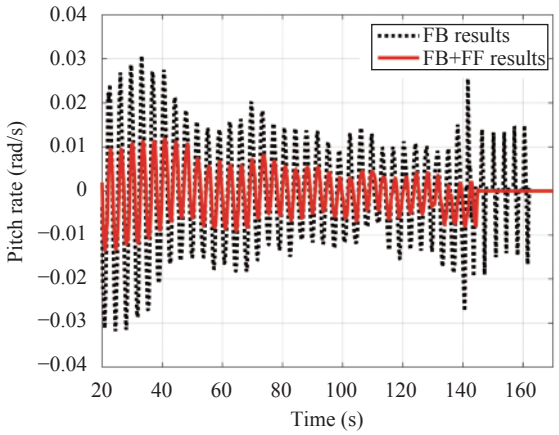

Fig. 13 Comparison of the pitch activity (mean wind 12 m/s, the dotted line represents the baseline feedback (FB) controller, the solid line represents the combined feedforward (FF) and FB controller).

tension of the pitch actuator. Switching from the above rated wind condition to the below rated condition can be observed in Fig. 13. In below rated operation, the pitching is fixed, thus the pitch rate is 0.

With the proposed method, the reduction in the rotor torque and the tower acceleration are presented in Figs. 14–19.

Fig. 14 shows the alleviation of the out-of-plane rotor torque fluctuations, and the reduction in the frequency domain can be seen in Fig. 15. These demonstrate the improvements on rotor load reduction in the out-of-plane direction. Similar results on in-plane rotor load reduction are shown in Figs. 16 and 17.

The considerable reductions in Figs. 18 and 19 represent a much smaller tower movements in the fore-aft direction.

As a significant part of wind turbine performance, the effect on the power output is also examined. As shown in Fig. 20, the power fluctuations are slightly reduced, but not much affected by the LIDAR-assisted feedforward channel.

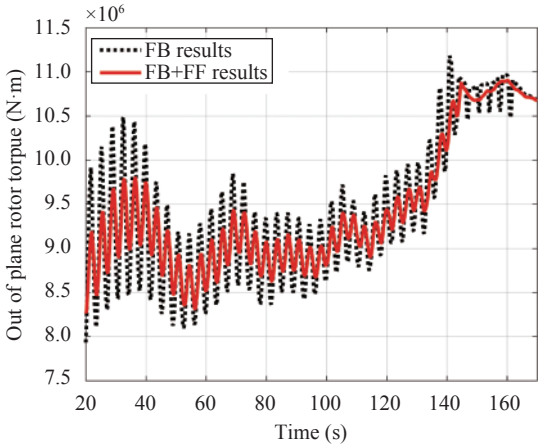

Fig. 14 Comparison of the out of plane rotor torque (mean wind 12 m/s)

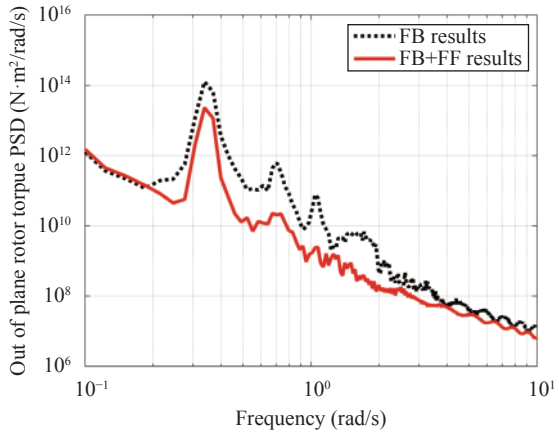

Fig. 15 PSD of the out of plane rotor torque (mean wind 12 m/s)

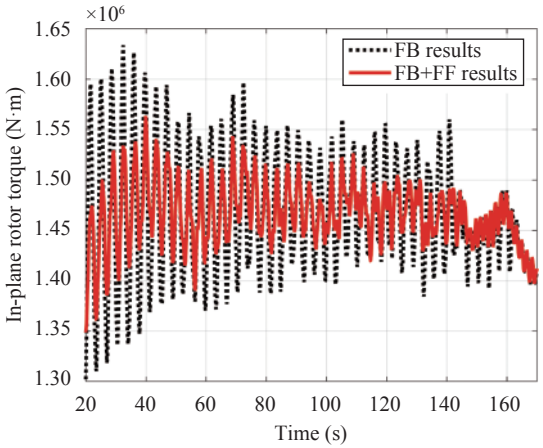

Fig. 16 Comparison of the in-plane rotor torque (mean wind 12 m/s)

4.2 High wind speed region

A turbulent wind with mean wind speed of 20 m/s and

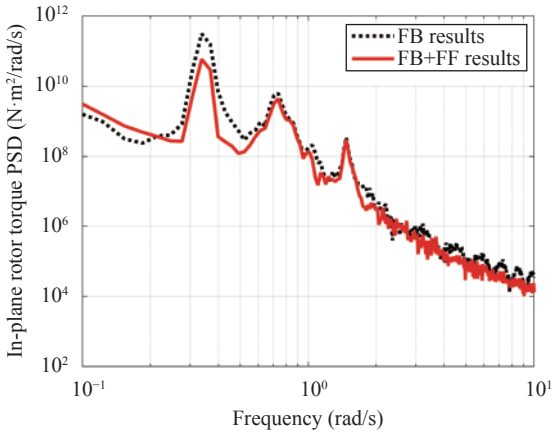

Fig. 17 PSD of the in-plane rotor torque (mean wind 12 m/s)

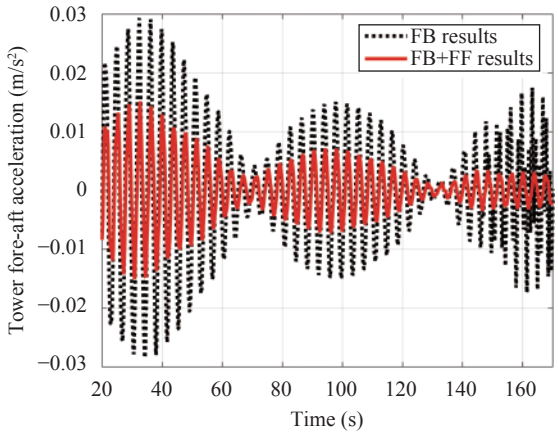

Fig. 18 Comparison of the tower fore-aft acceleration (mean wind 12 m/s)

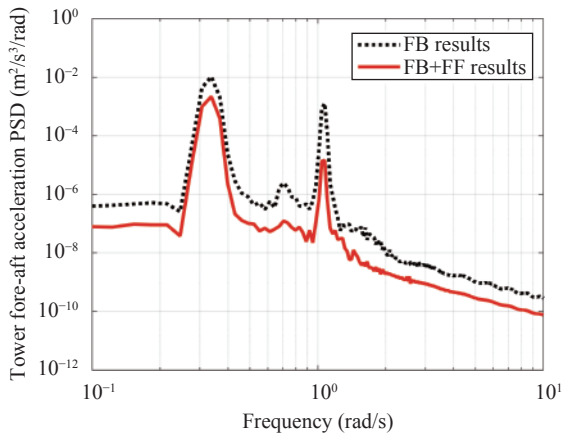

Fig. 19 PSD of the tower fore-aft acceleration (mean wind 12 m/s)

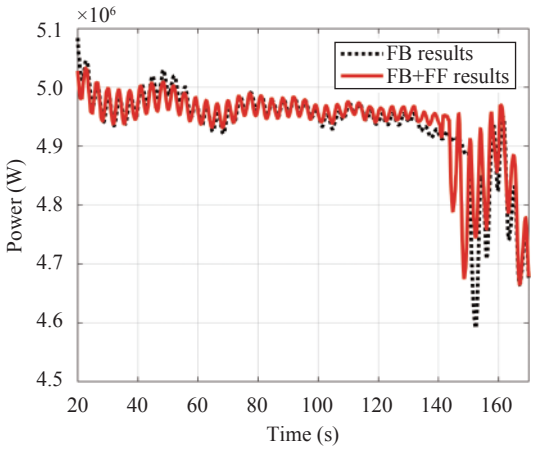

Fig. 20 Comparison of the power output (mean wind 12 m/s)

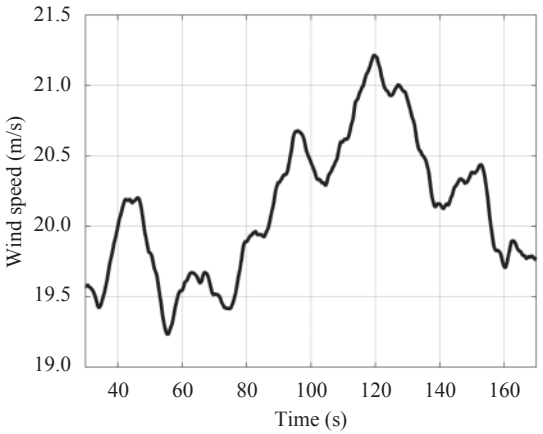

Fig. 21 Wind speed used in the high wind speed region (mean wind 20 m/s, turbulence intensity 5%)

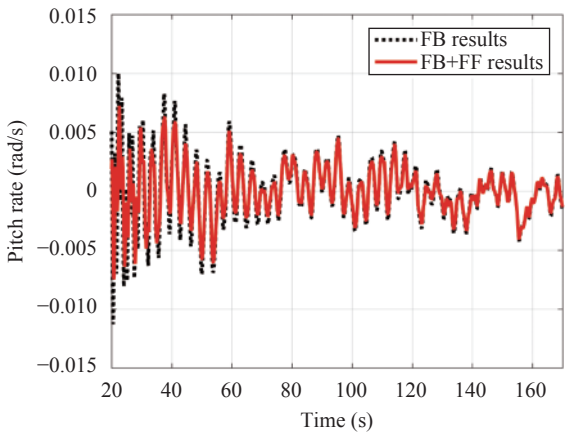

Fig. 22 Comparison of the pitch rate (mean wind 20 m/s)

turbulence intensity of 5% is selected representing a high wind speed region, as shown in Fig. 21.

Simulation results in high wind speed region shown in Figs. 22–28 also demonstrate the reduction in the pitch variations, the rotor loads and the tower loads when using the proposed method.

The out-of-plane rotor torque is shown in Fig. 23, where the load reduction performance is not as obvious as that in the transition region. But the reduction on rotor loads can still be observed in Fig. 24 at specific peaks.

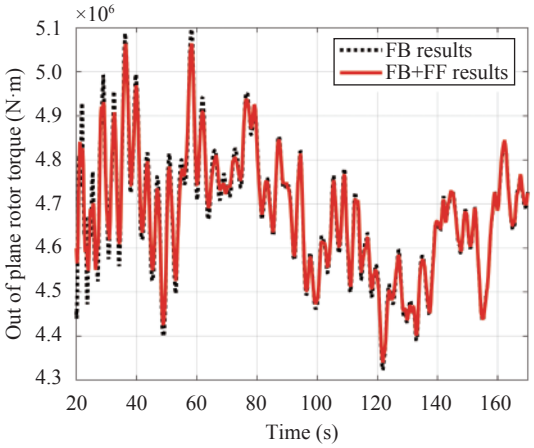

Fig. 23 Comparison of the out of plane rotor torque (mean wind 20 m/s)

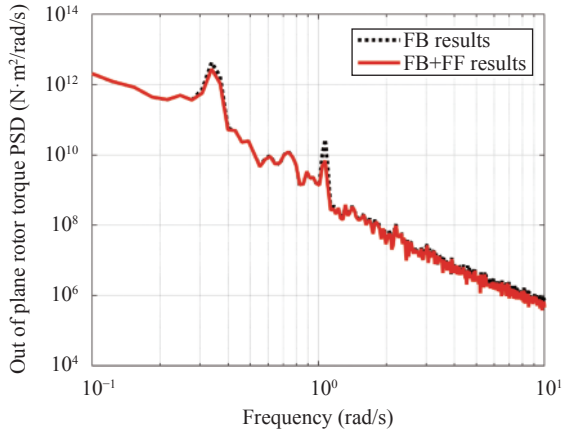

Fig. 24 PSD of the out of plane rotor torque (mean wind 20 m/s)

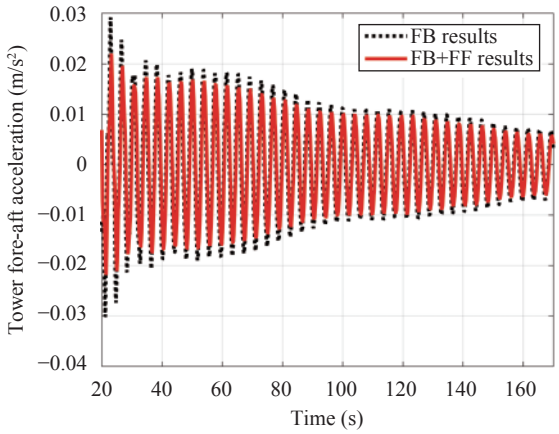

Fig. 25 Comparison of the tower fore-aft acceleration (mean wind 20 m/s)

Similarly, results on tower load reduction are shown in Figs. 25–28. The results of the combined feedforward/feedback controller do not show apparent differences compared with the baseline feedback controller in high wind speed region. Only small improvements on both rotor and tower load reductions can be observed.

Finally, Fig. 29 shows the results on power output, from which it is validated that the added feedforward channel does not affect the power generation as expected.

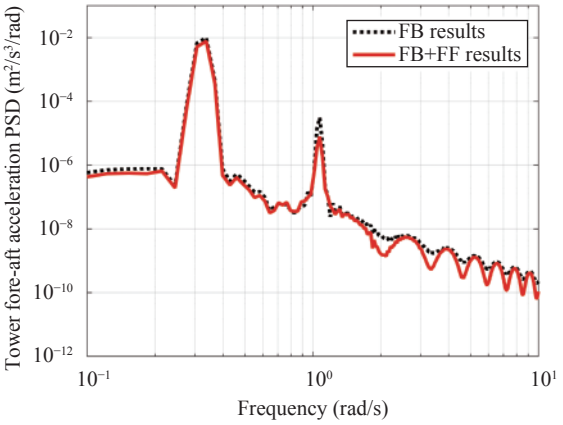

Fig. 26 PSD of the tower fore-aft acceleration (mean wind 20 m/s)

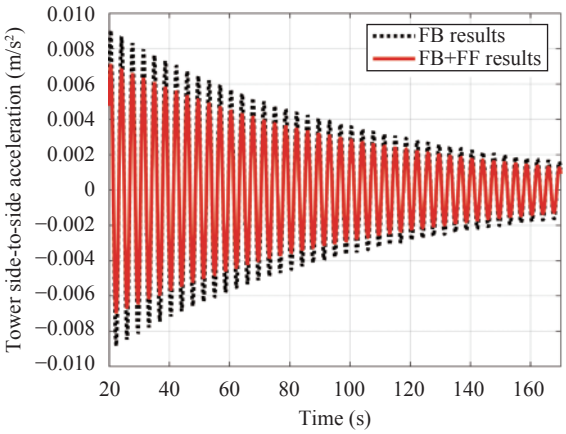

Fig. 27 Comparison of the tower side-to-side acceleration (mean wind 20 m/s)

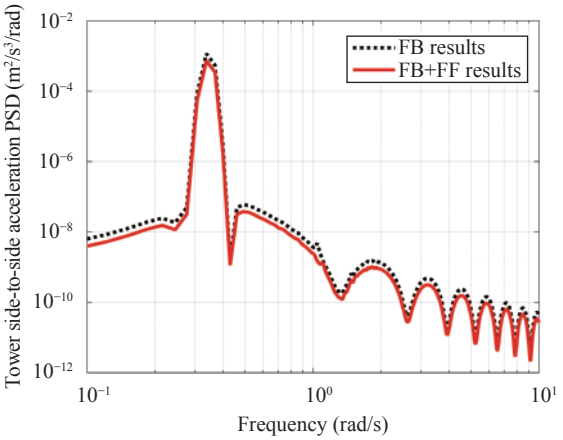

Fig. 28 PSD of the tower side-to-side acceleration (mean wind 20 m/s)

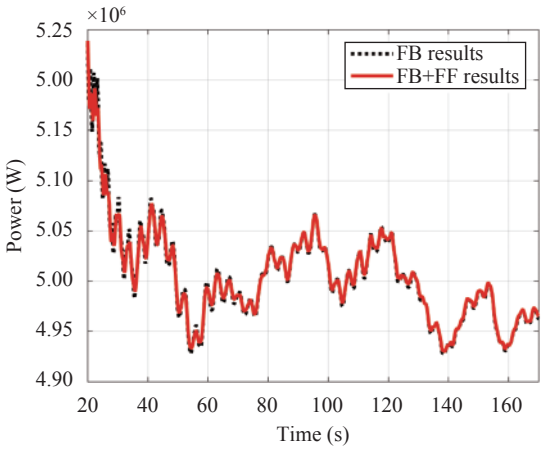

Fig. 29 Comparison of the power output (mean wind 20 m/s)

5 Conclusions

In this work, the information of LIDAR wind measurement is explored in controller design for large wind turbine systems with a focus on reducing structural loads on rotor and tower. A combined feedforward/feedback controller is established in which the feedforward channel is designed based on the preview wind information from pseudo-LIDAR measurement.

The original baseline control system has its own load reduction design, i.e., the drive-train filter for drive train load reduction, and the tower feedback loop for tower load reduction. With the augmented feedforward control, further load reductions on rotor and tower can be achieved. These improvements could also influence the drive-train components, since the rotor loads will propagate down to the drive-train. As a result, the fatigue loads on the wind turbine could be reduced leading to an extended lifetime and reduced maintenance cost. Moreover, the reduction on pitch variations is also achieved indicating a less aggressive pitch actuator activity. Finally, it can be observed that the power generation performance is not much affected by the proposed control method. Compared to the results in high wind speed region, the combined controller shows more clear improvements, in the transition region, on pitch activities and load reduction performance.

The modern measurement technique of LIDAR provides comprehensive and more accurate information on wind speed in a wide changing wind field. From the controller design point of view, this improved measurement provides the opportunity of taking preview wind information into the controller design. The performance of the developed control system largely depends on the proper use of such preview wind information. It is therefore crucial to develop a working model of wind evolution using the LIDAR measurement, which is a challenging task due to the complex and changing behavior of wind. Another vital factor is how to extract reliable wind speed information from the real LIDAR measurement. This can perhaps be progressed through more systematic data processing of the collected multi-channel data.

Appendix

In the simulation study, there are six operating points selected in the wind speed region of [12, 22] m/s with an interval of 2 m/s. The transfer functions between the wind speed and the generator speed, $G_{v\omega}$, at the six selected operating points are given as follows.

$$G_{v\omega 12} = \frac{0.000\,178\,7s^7 + 0.012\,59s^6 + 1.17s^5 + 147.2s^4 + 36.01s^3 + 4\,441s^2 + 183.8s + 1.17 \times 10^4}{s^7 + 4.722s^6 + 110.2s^5 + 366.6s^4 + 2\,241s^3 + 1\,566s^2 + 5\,620s + 353.9}$$

$$G_{v\omega 14} = \frac{0.000\,187\,7s^7 + 0.011\,61s^6 + 1.039s^5 + 130.2s^4 + 36.3s^3 + 4\,631s^2 + 193.1s + 1.24 \times 10^4}{s^7 + 4.572s^6 + 110.1s^5 + 354.9s^4 + 2\,244s^3 + 1\,609s^2 + 5\,619s + 623.9}$$

$$G_{v\omega 16} = \frac{0.000\,206\,3s^7 + 0.011\,78s^6 + 1.019s^5 + 127.3s^4 + 39.06s^3 + 5\,027s^2 + 211.6s + 1.358 \times 10^4}{s^7 + 4.563s^6 + 110.2s^5 + 355.4s^4 + 2\,260s^3 + 1\,729s^2 + 5\,662s + 979.8}$$

$$G_{v\omega 18} = \frac{0.000\,230\,3s^7 + 0.012\,48s^6 + 1.047s^5 + 130.5s^4 + 42.65s^3 + 5\,531s^2 + 233.9s + 1.502 \times 10^4}{s^7 + 4.604s^6 + 110.4s^5 + 360.6s^4 + 2\,281s^3 + 1\,893s^2 + 5\,724s + 1\,414}$$

$$G_{v\omega 20} = \frac{0.000\,255\,2s^7 + 0.013\,28s^6 + 1.085s^5 + 135.2s^4 + 45.83s^3 + 6\,013s^2 + 254.2s + 1.639 \times 10^4}{s^7 + 4.609s^6 + 110.6s^5 + 362.8s^4 + 2\,305s^3 + 2\,057s^2 + 5\,798s + 1\,882}$$

$$G_{v\omega 22} = \frac{0.000\,28s^7 + 0.014\,09s^6 + 1.125s^5 + 140.2s^4 + 48.61s^3 + 6\,465s^2 + 272.5s + 1.767 \times 10^4}{s^7 + 4.598s^6 + 110.8s^5 + 363.8s^4 + 2\,332s^3 + 2\,225s^2 + 5\,879s + 2\,379}.$$

The transfer functions between the pitch demand and generator speed $G_{\beta\omega}$, at the six operating points are given as follows.

$$G_{\beta\omega 12}=\frac{-0.65s^7-116.4s^6+466.9s^5-5\,082s^4+1.4\times10^4s^3-8.53\times10^4s^2+6.46\times10^4s-2.09\times10^5}{s^7+4.702s^6+110.6s^5+365.2s^4+2\,275s^3+1\,563s^2+5\,710s+359.6}$$

$$G_{\beta\omega 14}=\frac{-0.539\,6s^7-90.7s^6-370s^5-5\,362s^4+9\,570s^3-1.419\times10^5s^2+4.451\times10^4s-3.714\times10^5}{s^7+4.55s^6+110.2s^5+353s^4+2\,254s^3+1\,602s^2+5\,642s+626.6}$$

$$G_{\beta\omega 16}=\frac{-0.467\,7s^7-77.47s^6-327.1s^5-5\,748s^4+7\,390s^3-1.864\times10^5s^2+3.446\times10^4s-4.973\times10^5}{s^7+4.545s^6+110.2s^5+353.9s^4+2\,264s^3+1\,723s^2+5\,671s+981.6}$$

$$G_{\beta\omega 18}=\frac{-0.418s^7-68.78s^6-304.3s^5-6\,343s^4+5\,822s^3-2.324\times10^5s^2+2.721\times10^4s-6.263\times10^5}{s^7+4.59s^6+110.4s^5+359.4s^4+2\,283s^3+1\,888s^2+5\,728s+1\,415}$$

$$G_{\beta\omega 20}=\frac{-0.383s^7-62.57s^6-287.6s^5-6\,943s^4+4\,499s^3-2.744\times10^5s^2+2.109\times10^4s-7.435\times10^5}{s^7+4.598s^6+110.6s^5+361.8s^4+2\,307s^3+2\,053s^2+5\,799s+1\,883}$$

$$G_{\beta\omega 22}=\frac{-0.356\,7s^7-57.83s^6-275.5s^5-7\,591s^4+3\,394s^3-3.166\times10^5s^2+1.592\times10^4s-8.609\times10^5}{s^7+4.589s^6+110.8s^5+363s^4+2\,333s^3+2\,222s^2+5\,878s+2\,380}.$$

The feedforward controllers developed at these operating points are described by a set of 6th-order transfer function models.

$$G_{FF12}=\frac{1.334s^4+56.7-3s^3+40.14s^2+0.78s+105.6}{s^6+4.09s^5+45.09s^4-126s^3+758.3s^2-580.3s+1\,860}$$

$$G_{FF14}=\frac{1.5s^4-0.01s^3+53.32s^2+1.02s+142.5}{s^6+3.94s^5+61.69s^4-118.9s^3+1\,627s^2-534.5s+4\,252}$$

$$G_{FF16}=\frac{1.72s^4-0.02s^3+67.59s^2+1.3s+182.3}{s^6+3.93s^5+77.47s^4-115.4s^3+2\,501s^2-506.4s+6\,664}$$

$$G_{FF18}=\frac{1.98s^4-0.02s^3+83.61s^2+1.62s+226.8}{s^6+3.98s^5+96.21s^4-112.2s^3+3\,509s^2-477.8s+9\,444}$$

$$G_{FF20}=\frac{2.25s^4-0.04s^3+99.69s^2+1.92s+271.4}{s^6+3.99s^5+115.6s^4-107.1s^3+4\,546s^2-440.3s+1.23\times10^4}$$

$$G_{FF22}=\frac{2.52s^4-0.05s^3+115.7s^2+2.21s+315.7}{s^6+3.98s^5+136.4s^4-102.2s^3+5\,663s^2-401.2s+1.54\times10^4}.$$

Open Access

References

[1] E. A. Bossanyi. The design of closed loop controllers for wind turbines. *Wind Energy*, vol. 3, no. 3, pp. 149163, 2000.DOI: 10.1002/(ISSN)1099-1824.

[2] W. E. Leithead, B. Connor. Control of variable speed wind turbines: Design task. *International Journal of Control*, vol. 73, no. 13, pp. 11891212, 2000.DOI: 10.1080/002071700417849.

[3] F. D. Bianchi, R. J. Mantz, H. De Battista. Wind Turbine Control Systems: Principles, Modelling and Gain Scheduling Design, London, UK: Springer-Verlag, 2007.

[4] E. A. Bossanyi. Wind turbine control for load reduction. *Wind Energy*, vol. 6, no. 3, pp. 229244, 2003.DOI: 10.1002/(ISSN)1099-1824.

[5] W. E. Leithead, S. Dominguez. Controller design for the cancellation of the tower fore-aft mode in a wind turbine. In *Proceedings of the 44th IEEE Conference on Decision and Control*, IEEE, Seville, Spain, pp. 12761281, 2005.

[6] W. E. Leithead, S. Dominguez, C. Spruce. Analysis of tower/blade interaction in the cancellation of the tower fore-aft mode via control. In *Proceedings of European Wind Energy Conference*, EWEA, London, UK, 2004.

[7] W. E. Leithead, S. Dominguez. Coordinated control design for wind turbine control systems. In *Proceedings of European Wind Energy Conference and Exhibition, University Strathclyde Glasgow*, Athens, Greece, vol. 3, pp. 18181825, 2006.

[8] E. A. Bossanyi. Individual blade pitch control for load reduction. *Wind Energy*, vol. 6, no. 2, pp. 119128, 2003.DOI: 10.1002/(ISSN)1099-1824.

[9] Y. Han, W. E. Leithead. Combined wind turbine fatigue and ultimate load reduction by individual blade control. *Journal of Physics*: *Conference Series*, vol. 524, no. 1, Article number 012062, 2014. DOI: 10.1088/1742-6596/524/1/012062.

[10] M. Harris, M. Hand, A. Wright. Lidar for Turbine Control, Technical Report NREL/TP-500-39154, National Renewable Energy Laboratory, Golden, USA, 2006.

[11] N. Angelou, T. Mikkelsen, K. H. Hansen, M. Sjholm, M. Harris. LIDAR wind speed measurements from a rotating spinner. In *Proceedings of European Wind Energy Conference and Exhibition*, EWEA, Warsaw, Poland, 2010.

[12] M. Sjholm, T. Mikkelsen, J. Mann, K. Enevoldsen, M. Courtney. Spatial averaging-effects on turbulence measured by a continuous-wave coherent lidar. *Meteorologische Zeitschrift*, vol. 18, no. 3, pp. 281287, 2009.DOI: 10.1127/0941-2948/2009/0379.

[13] D. A. Smith, M. Harris, A. S. Coffey, T. Mikkelsen, H. E. Jrgensen, J. Mann, R. Danielian. Wind lidar evaluation at the Danish wind test site in Hvsre. *Wind Energy*, vol. 9, no. 12, pp. 8793, 2006.DOI: 10.1002/(ISSN)1099-1824.

[14] D. Schlipf, M. Khn. Prospects of a collective pitch control by means of predictive disturbance compensation assisted by wind speed measurements. In *Proceedings of the 9th German Wind Energy Conference*, EWEA, Bremen, Germany, 2008.

[15] D. Schlipf, E. Bossanyi, C. E. Carcangiu, T. Fischer, T. Maul, M. Rossetti. LIDAR Assisted Collective Pitch Control, Technical Report UpWind Deliverable D5.1.3, the European Wind Energy Association (EWEA), Stuttgart, Germany, 2010.

[16] J. Laks, L. Pao, A. Wright. Combined feed-forward/feedback control of wind turbines to reduce blade flap bending moments. In *Proceedings of the 47th AIAA Aerospace Sciences Meeting including The New Horizons Forum and Aerospace Exposition*, AIAA, Orlando, USA, 2009.

[17] F. Dunne, D. Schlipf, L. Y. Pao, A. D. Wright, B. Jonkman, N. Kelley, E. Simley. Comparison of two independent lidar-based pitch control designs. In *Proceedings of 50th AIAA Aerospace Sciences Meeting Including the New Horizons Forum and Aerospace Exposition*, AIAA, Nashville, USA, 2012.

[18] F. Dunne, L. Y. Pao, A. D. Wright, B. Jonkman, N. Kelley. Adding feedforward blade pitch control to standard feedback controllers for load mitigation in wind turbines. *Mechatronics*, vol. 21, no. 4, pp. 682690, 2011.DOI: 10.1016/j.mechatronics.2011.02.011.

[19] J. Laks, L. Pao, A. Wright, N. Kelley, B. Jonkman. The use of preview wind measurements for blade pitch control. *Mechatronics*, vol. 21, no. 4, pp. 668681, 2011.DOI: 10.1016/j.mechatronics.2011.02.003.

[20] N. Wang, K. E. Johnson, A. D. Wright. FX-RLS-based feedforward control for LIDAR-enabled wind turbine load mitigation. *IEEE Transactions on Control Systems Technology*, vol. 20, no. 5, pp. 12121222, 2012.DOI: 10.1109/TCST.2011.2163515.

[21] J. Laks, L. Y. Pao, E. Simley, A. Wright, N. Kelley, B. Jonkman. Model predictive control using preview measurements from lidar. In *Proceedings of the 49th Aerospace Sciences Meeting Including the New Horizons Forum and Aerospace Exposition*, AIAA, Orlando, IEEE, USA, 2011.

[22] D. Schlipf, L. Y. Pao, P. W. Cheng. Comparison of feedforward and model predictive control of wind turbines using LIDAR. In *Proceedings of the 51st Conference on Decision and Control*, IEEE, Maui, USA, pp. 30503055, 2012.

[23] D. Schlipf, D. J. Schlipf, M. Khn. Nonlinear model predictive control of wind turbines using LIDAR. *Wind Energy*, vol. 16, no. 7, pp. 11071129, 2013.DOI: 10.1002/we.v16.7.

[24] A. Scholbrock, P. Fleming, L. Fingersh, A. Wright, D. Schlipf, F. Haizmann, F. Belen. Field testing LIDAR-based feed-forward controls on the NREL controls advanced research turbine. In *Proceedings of the 51st AIAA Aerospace Sciences Meeting Including the New Horizons Forum and Aerospace Exposition*, AIAA, Grapevine, Texas, USA, 2013.

[25] D. Schlipf, P. Fleming, F. Haizmann, A. Scholbrock, M. Hofsss, A. Wright, P. W. Cheng. Field testing of feedforward collective pitch control on the CART2 using a nacelle-based lidar scanner. *Journal of Physics: Conference Series*, vol. 555, no. 1, Article number 012090, 2014.

[26] F. Haizmann, D. Schlipf, S. R, A. S, A. W, C. Slinger, J. Medley, M. Harris, E. Bossanyi, P. W. Cheng. Optimization of a feed-forward controller using a CW-lidar system on the CART3. In *Proceedings of American Control Conference*, IEEE, Chicago, USA, pp. 37153720, 2015.

[27] N. Wang, K. E. Johnson, A. D. Wright. Comparison of strategies for enhancing energy capture and reducing loads using LIDAR and feedforward control. *IEEE Transactions on Control Systems Technology*, vol. 21, no. 4, pp. 11291142, 2013.DOI: 10.1109/TCST.2013.2258670.

[28] D. Schlipf, S. Kapp., J. Anger, O. Bischoff, M. Hofsss, A. Rettenmeier, M. Khn. Prospects of optimization of energy production by lidar assisted control of wind turbines. In *Proceedings of European Wind Energy Association Annual Event*, EWEA, Brussels, Belgium, 2011.

[29] E. A. Bossanyi, A. Kumar, O. Hugues-Salas. Wind turbine control applications of turbine-mounted LIDAR. *Journal of Physics*: *Conference Series*, vol. 555, no. 1, Article number 012011, 2014. DOI: 10.1088/1742-6596/555/1/012011.

[30] E. Simley, L. Y. Pao, R. Frehlich, B. Jonkman, N. Kelley. Analysis of wind speed measurements using continuous wave LIDAR for wind turbine control. In *Proceedings of 49th Aerospace Sciences Meeting including the New Horizons Forum and Aerospace Exposition*, AIAA, Orlando, USA, 2011.

[31] E. Bossanyi. Un-freezing the turbulence: Application to LiDAR-assisted wind turbine control. *IET Renewable Power Generation*, vol. 7, no. 4, pp. 321329, 2013.DOI: 10.1049/iet-rpg.2012.0260.

[32] D. Schlipf, P. W. Cheng, J. Mann. Model of the correlation between lidar systems and wind turbines for lidar-assisted control. *Journal of Atmospheric and Oceanic Technology*, vol. 30, no. 10, pp. 22332240, 2013.DOI: 10.1175/JTECH-D-13-00077.1.

[33] E. Simley, L. Y. Pao. A longitudinal spatial coherence model for wind evolution based on large-eddy simulation. In *Proceedings of American Control Conference*, IEEE, Chicago, USA, pp. 37083714, 2015.

[34] J. Laks, E. Simley, L. Pao. A spectral model for evaluating the effect of wind evolution on wind turbine preview control. In *Proceedings of American Control Conference*, IEEE, Washington, USA, pp. 36733679, 2013.

[35] E. Simley, L. Pao. Reducing LIDAR wind speed measurement error with optimal filtering. In *Proceedings of American Control Conference*, IEEE, Washington DC, USA, pp. 621627, 2013.

[36] F. Dunne, L. Y. Pao, D. Schlipf, A. K. Scholbrock. Importance of lidar measurement timing accuracy for wind turbine control. In *Proceedings of American Control Confer-*

ence, IEEE, Portland, USA, pp. 37163721, 2014.

[37] E. Simley, N. Angelou, T. Mikkelsen, M. Sjholm, J. Mann, L. Y. Pao. Characterization of wind velocities in the upstream induction zone of a wind turbine using scanning continuous-wave lidars. *Journal of Renewable and Sustainable Energy*, vol. 8, no. 1, Article number 013301, 2016.

[38] J. Bao, H. Yue, W. E. Leithead, J. Q. Wang. LIDAR-assisted wind turbine gain scheduling control for load reduction. In *Proceedings of the 22nd International Conference on Automation and Computing*, IEEE, Colchester, UK, pp. 1520, 2016.

[39] P. S. Veers. Three-dimensional Wind Simulation, Technical Report SAND-88-0152, Sandia National Labs., Albuquerque, USA, 1988.

[40] W. E. Leithead and B. Connor. Control of variable speed wind turbines: Dynamic models. *International Journal of Control*, vol. 73, no. 13, pp. 11731188, 2000.DOI: 10.1080/002071700417830.

[41] W. E. Leithead, D. J. Leith, F. Hardan, H. Markou. Global gain-scheduling control for variable speed wind turbines. In *Proceedings of European Wind Energy Conference*, EWEA, Nice, France, pp. 853856, 1999.

[42] M. Tomizuka. Zero phase error tracking algorithm for digital control. *Journal of Dynamic Systems, Measurement, and Control*, vol. 109, no. 1, pp. 6568, 1987.DOI: 10.1115/1.3143822.

[43] H. Romdhane, K. Dehri, A. S. Nouri. Second order sliding mode control for discrete decouplable multivariable systems via input-output models. *International Journal of Automation and Computing*, vol. 12, no. 6, pp. 630638, 2015.DOI: 10.1007/s11633-015-0904-z.

[44] R. Garraoui, M. Ben Hamed, L. Sbita. A robust optimization technique based on first order sliding mode approach for photovoltaic power systems. *International Journal of Automation and Computing*, vol. 12, no. 6, pp. 620629, 2015.DOI: 10.1007/s11633-015-0902-1.

[45] Z. Q. Wu, J. P. Xie. Design of adaptive robust guaranteed cost controller for wind power generator. *International Journal of Automation and Computing*, vol. 10, no. 2, pp. 111117, 2013.DOI: 10.1007/s11633-013-0703-3.

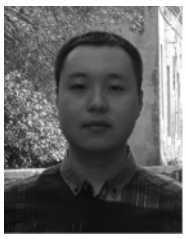

Jie Bao received the B. Sc. and M. Sc. degrees in electronic and electrical engineering from the University of Strathclyde, UK in 2011 and 2012, respectively. He is currently a Ph. D. degree candidate at the same university.

His research interests include modelling and control of wind turbine systems with a focus on LIDAR-based technology in wind energy systems.

E-mail: jie.bao@strath.ac.uk

ORCID iD: 0000-0001-8967-0729

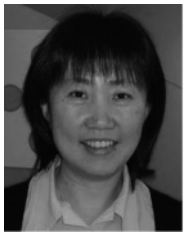

Hong Yue received the B. Eng. and M. Sc. degrees in process control engineering from Beijing University of Chemical Technology, Beijing, China in 1990 and 1993, respectively, and the Ph. D. degree in control theory and applications from East China University of Science and Technology, China in 1996. She is a senior lecturer at the Wind Energy and Control Centre, Department of Electronic and Electrical Engineering, University of Strathclyde, UK.

Her research interests include modelling, control and optimization of complex systems including power and wind energy systems, process systems, biological and biochemical networks.

E-mail: hong.yue@strath.ac.uk (Corresponding author)

ORCID iD: 0000-0003-2072-6223

William E. Leithead received the B. Sc. degree in mathematical physics and the Ph. D. degree in theoretical physics from the University of Edinburgh, UK in 1971 and 1976, respectively. He is the head of the Wind Energy and Control Centre at the University of Strathclyde, UK. He is the director of the Engineering and Physical Sciences Research Council (EPSRC) for Doctoral Training in wind and marine energy systems, and is the chair of the EPSRC Supergen Wind Hub. He is a member of the European Energy Research Alliance Joint Programme Wind Steering Committee, the European Academy of Wind Energy Executive Committee, the Scientific Advisory Board of the Norwegian Centre for Offshore Wind Technology (Bergen), and is the deputy chair of the ORE Catapult Research Advisory Group. He has been awarded more than 60 research grants and is the author of more than 250 academic publications.

His research interests include control engineering and wind energy systems with particular focus on the conceptual design of wind turbines and wind turbine and farm control system design.

E-mail: w.leithead@strath.ac.uk

Ji-Qiang Wang received the B. Sc. degree in industrial engineering & management, both from Xi′an Jiaotong University, China in 2003, received the Ph.D. degree from the University of Sheffield, UK in 2008. He is currently an associate professor at Nanjing University of Aeronautics & Astronautics, China, after a research fellowship at the University of Strathclyde, UK in 2009.

His research interests include nonlinear control, vibration control and aircraft engine control.

E-mail: jiqiang.wang@nuaa.edu.cn